PLOS ONE

RESEARCH ARTICLE

Position of rhodopsin photoisomerization on the disk surface confers variability to the rising phase of the single photon response in vertebrate rod photoreceptors

Giovanni Caruso[1]*, Colin J. Klaus[2], Heidi E. Hamm[3], Vsevolod V. Gurevich[3], Clint L. Makino[4], Emmanuele DiBenedetto[5]

1 Italian National Research Council, Istituto di Scienze del Patrimonio Culturale, Roma, Italy, **2** The Mathematical Biosciences Institute, Ohio State University, Columbus, OH, United States of America, **3** Department of Pharmacology, Vanderbilt University Medical Center, Nashville, TN, United States of America, **4** Department of Physiology & Biophysics, Boston University School of Medicine, Boston, MA, United States of America, **5** Department of Mathematics, Vanderbilt University, Nashville, TN, United States of America

* giovanni.caruso@cnr.it

Citation: Caruso G, Klaus CJ, Hamm HE, Gurevich VV, Makino CL, DiBenedetto E (2020) Position of rhodopsin photoisomerization on the disk surface confers variability to the rising phase of the single photon response in vertebrate rod photoreceptors. PLoS ONE 15(10): e0240527. https://doi.org/10.1371/journal.pone.0240527

Editor: Karl-Wilhelm Koch, Carl von Ossietzky Universitat Oldenburg, GERMANY

Received: May 17, 2020

Accepted: September 29, 2020

Published: October 14, 2020

Data Availability Statement: The finite element code for the model is posted on Zenodo (doi:10.5281/zenodo.3334503). The model itself and the parameter sets appear in the text and in Supporting Information.

Funding: DMS 1812601 (GC, VVG, CJK, HEH, CLM, ED); the National Institute of General Medical Sciences: GM122491 (VVG); the National Eye Institute: EY06062 (HEH), EY 10291 (HEH), EY011500 (VVG), EY031702 (CLM); the Cornelius

Abstract

Retinal rods function as accurate photon counters to provide for vision under very dim light. To do so, rods must generate highly amplified, reproducible responses to single photons, yet outer segment architecture and randomness in the location of rhodopsin photoisomerization on the surface of an internal disk introduce variability to the rising phase of the photon response. Soon after a photoisomerization at a disk rim, depletion of cGMP near the plasma membrane closes ion channels and hyperpolarizes the rod. But with a photoisomerization in the center of a disk, local depletion of cGMP is distant from the channels in the plasma membrane. Thus, channel closure is delayed by the time required for the reduction of cGMP concentration to reach the plasma membrane. Moreover, the local fall in cGMP dissipates over a larger volume before affecting the channels, so response amplitude is reduced. This source of variability increases with disk radius. Using a fully space-resolved biophysical model of rod phototransduction, we quantified the variability attributable to randomness in the location of photoisomerization as a function of disk structure. In mouse rods that have small disks bearing a single incisure, this variability was negligible in the absence of the incisure. Variability was increased slightly by the incisure, but randomness in the shutoff of rhodopsin emerged as the main source of single photon response variability at all but the earliest times. Variability arising from randomness in the transverse location of photoisomerization increased in magnitude and persisted over a longer period in the photon response of large salamander rods. A symmetric arrangement of multiple incisures in the disks of salamander rods greatly reduced this variability during the rising phase, but the incisures had the opposite effect on variability arising from randomness in rhodopsin shutoff at later times.

Vanderbilt Chair (VVG) and The Mathematics Biosciences Institute (CJK) which is funded by the National Science Foundation DMS 1440386. The funders had no role in study design, data collection and analysis, decision to publish, or preparation of manuscript. The contents reported herein are those of the authors and do not necessarily express the official views of the National Science Foundation or the National Institutes of Health.

Competing interests: The authors have declared that no competing interests exist.

Introduction

In the vertebrate retina, rod photoreceptors provide visual input under very dim light. The conversion of light into an electrical signal occurs within a specialized cilium called the outer segment. Therein hundreds to thousands of flattened disks whose membranous surfaces are densely packed with rhodopsin, capture photons efficiently (Fig 1). Photoisomerization of rhodopsin initiates a G protein cascade restricted to one face of a disk, that culminates in the hydrolysis of cGMP by activated phosphodiesterase (PDE*). The ensuing fall in cGMP concentration in the cytosolic volume between disks that propagates to their rims closes cyclic nucleotide gated (CNG) channels in the plasma membrane (reviewed in [1, 2]). The subsequent reduction in an inward current carried by Na^+ and Ca^{2+} through the channel hyperpolarizes the membrane. The single photon response (SPR) builds relatively slowly because amplification in this cascade takes time, but downstream rod "ON" bipolar cells improve upon temporal resolution by signaling on a faster time scale [3, 4]. Thus, it appears that for the single photon response, or more generally for very dim illumination levels, the rising phase of the rod response is most critical for vision.

The SPR must be reproducible to carry meaningful information about light intensity. Rhodopsin is activated by photoisomerization of its covalently attached chromophore, 11-*cis* retinal, which is converted to all-*trans* retinal. A major source of variability affecting the peak and recovery phase of the SPR originates from randomness in the inactivation of photoexcited rhodopsin, R* [9–11]. R* is phosphorylated (up to 6 or 7 times in different species) with a variable delay separating the addition of each phosphate, and by the subsequent binding of arrestin-1 (a.k.a. visual or rod arrestin), which is dependent upon the number of phosphates added [12]. Progressive phosphorylation reduces R* activity [13, 14], but arrestin-1 binding is necessary for complete quench [15]. However, randomness in R* shutoff does not greatly affect the early

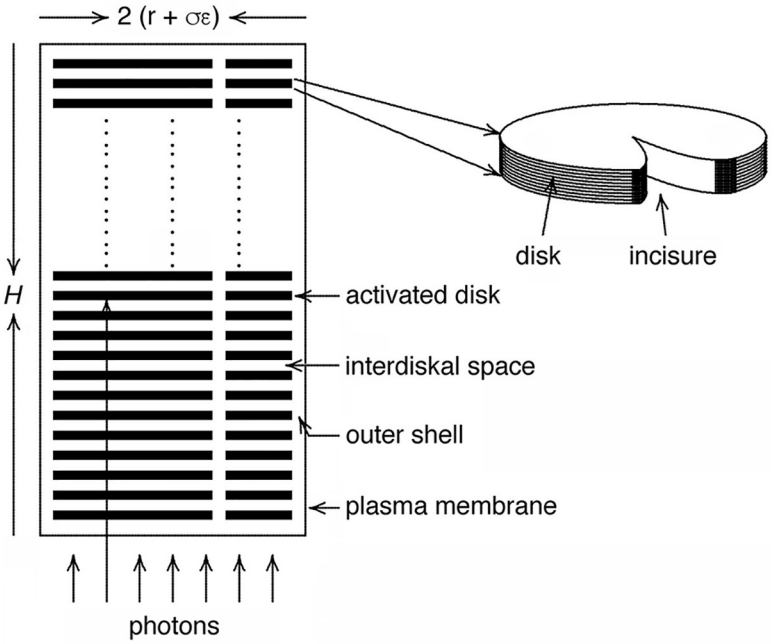

Fig 1. Disk barriers to the axial diffusion of cGMP and Ca^{2+} in the rod outer segment. Membranous disks of radius r segment the cytoplasm into layers of interdiskal space, 14.5 nm in thickness. Layers are interconnected by an outer shell of thickness σε that separates the disks from the plasma membrane, as well as by the single incisure in each mouse rod disk (as shown) and the multiple incisures in each salamander rod disk. In mouse, the outer segment diameter = 2 (r + σε) is ~1.4 μm [5], whereas in salamander, it is typically 10–12 μm [6, 7], but it can be as large as 13 μm [8].

https://doi.org/10.1371/journal.pone.0240527.g001

rising phase of the response since it is unlikely that the first phosphorylation of R^* will have even occurred during that time [16, 17]. A potentially important source of variability during this period arises from randomness in the location of the rhodopsin photoisomerization on the disk [18, 19]. Rhodopsin, visual G protein transducin, and PDE are anchored in the membranes of internal disks in the rod outer segment. Following photon absorption by a rhodopsin molecule at the disk rim, activation of the first PDE produces a local depletion of cGMP in the cytosol in proximity to the CNG channels localized in the plasma membrane. Channel closure is relatively fast and vigorous. In contrast, the response to a photoisomerization at the center of the disk, i.e. farthest from the channels, is delayed as the local reduction in cGMP level in the cytoplasm between adjacent disks spreads and dissipates radially and through incisures axially, before finally impacting the CNG channels [20]. The delay will be brief if disk radius is small, but will be extended by an increase in disk size. Closure of the CNG channels reduces the concentration of Ca^{2+} in the cytoplasm. The reduction of Ca^{2+} leads to its replacement with Mg^{2+} on GCAPs, converting them from inhibitors to activators of guanylyl cyclase, which replenishes cGMP, leading to the opening of CNG channels, thereby terminating the signal.

Randomness in the spatiotemporal fall in cGMP due to R^* location wanes in importance over time as PDE^*s spread across the disk surface and cGMP diffuses throughout the outer segment, eventually yielding to randomness in R^* inactivation as the main source of SPR variability. Despite the importance of the rising phase of the SPR to visual signaling, little is known about the relative contribution of each source of variability and about the time when the transition in dominance occurs. Here, we explore these issues with a fully space-resolved biophysical model of phototransduction that accounts for radial as well as longitudinal diffusion of cGMP and Ca^{2+}. We used the model to evaluate different sources of variability, in isolation or in combinations, of the rising phase of the photon response. Since variability due to the location of photoisomerization should depend on disk size, we systematically varied disk radius and also applied the model to rods of salamander and mouse, whose disk radii differ by almost an order of magnitude [5, 8]. Disks in mouse rods have a single incisure [5, 21], whereas disks in salamander rods are partitioned by numerous incisures [8]. Incisures affect the movement of rhodopsin, transducin, and PDE on the disk membrane surface and also promote the axial diffusion of cGMP and Ca^{2+} in the cytosol, so some simulations were performed for both salamander and mouse rods in which the incisures were "removed" to test their function.

Methods

The fully space-resolved model of phototransduction was used with different parameter sets for salamander rods and for mouse rods. The model described previously [11, 18, 20, 22, 23] and parameter sets, similar to those in [19, 20, 22, 24] but with minor computational adjustments, are included as **S1 Appendix**, for completeness. These parameters and the formalism describe the independent activation of individual catalytic subunits of the PDE dimer by single transducins. The requirement for two transducins to simultaneously bind the PDE dimer before there is any significant activation [25] was tested in additional simulations. Our approach of using the heat equation as the solution for the spread of PDE activation across the disk surface [26] applies to both scenarios, as is shown below and in **S1 File**. The results presented below were obtained from the finite element code in Matlab format, accessible on Github (doi: 10.5281/zenodo.3334503), with the parameters specified in **S1 Appendix**. Some parameter substitutions were made for selected simulations to test specific hypotheses on the effect of incisures, disk radius and diffusion coefficient, as described in the text.

Each simulation was initiated by the creation of an R^* in the central disk of the outer segment, so any variability arising from differences in SPRs elicited at the proximal and distal

disks [27–30] was not tested. The site of rhodopsin activation was fixed on the disk surface at one of three specified positions for some simulations or at a random location to test for a role of its position on SPR variability. In the homogenized model, the outer segment was subdivided into three domains: the outer shell (treated as a cylindrical surface), the interior volume (a cylinder) and the special disk (disk containing the photoisomerized rhodopsin). The mesh of the outer shell used quadrilateral elements, the mesh of the interior volume employed prisms and the mesh of the special disk employed triangular elements. Linear shape functions mapped the unknowns inside each element in terms of their nodal values. A refinement along the axial direction around the activated disk level was adopted to account for the large axial gradients occurring there. A standard iso-parametric map was used to map the elements in the actual geometry into corresponding reference elements. Boundary conditions were enforced at each end of the interior volume and of the cylindrical outer shell and it was assumed that there was no axial flux of transduction proteins.

Shutoff of R^* activity proceeded with step-wise decrements in activity, each activity state having its own duration, according to the solution of a continuous time Markov chain [11]. For simulations probing the randomness in R^* shutoff, the duration of each R^* state had an exponential distribution with a mean found from curve fitting (see **S2, S4 Tables** in **S1 Appendix**). In all other simulations, R^* shutoff was deterministic, with the duration of each activity state assigned to the mean value for that state. For salamander, the average durations of the phosphorylated states were (s): 0.0833, 0.1000, 0.1250, 0.0625, 0.0714, 0.0833, and 0.1000, with an average R^* lifetime of 0.4 s. For mouse, the average durations were (s): 0.0159, 0.0190, 0.0238, 0.0109, 0.0123, 0.0142, and 0.0167, with an average R^* lifetime of 0.08 s.

The behavior of the CNG channels was modeled as a population. This decision was justified by the channel's low unitary conductance under physiological conditions, coupled with their high density (reviewed in [31]) and uniform axial distribution in the plasma membrane of the outer segment [32].

One thousand simulations were run for each set of parameters and conditions, after which the coefficient of variation (CV) was computed as the ratio of the standard deviation to the mean for the total influx of current into the rod outer segment (j_{tot}), carried by the CNG channels and the Na^+/K^+, Ca^{2+} exchanger. As will be discussed below, when assessing the variability at early times in the photon response, it was also useful to compute CV for the relative drop in current after photon absorption, $I(t) = 1 - j_{tot}/ j_{dark}$, where j_{dark} is the j_{tot} value in darkness.

Results

Effect of activation site on SPR variability

The first assessment of the impact of the location of rhodopsin activation on the SPR of a large salamander rod was made by comparing deterministic simulations for an R^* at each of three fixed positions on the disk surface: center of the disk, halfway between disk center and the rim, or at the rim. The spatiotemporal spread of transducin/PDE activation on the disk surface was modeled according to the diffusion of heat across a surface [26]. This approach yielded the average response to the photoisomerization at each location so that the effect of photoisomerization position could be assessed in isolation. Although randomness in the spatiotemporal pattern of PDE activation across the disk would confer additional variability in the rising phase of the SPR, its contribution to CV appears to be marginal [19]. The basal PDE activity was modeled as spatially uniform to remove confounding effects introduced by the discrete, spontaneous PDE activations that generate the continuous noise, cf. [33]. Disks in amphibian rods have multiple incisures that penetrate from the disk rim towards its center [8, 34, 35]. For simplicity and to isolate the effect of R^* position, the incisures were "removed" from the disks for the initial simulations.

Photoisomerization of a rhodopsin on the disk gave rise to striking radial gradients in cGMP that evolved and persisted throughout the duration of the photocurrent response (Fig 2). The form of the gradient varied markedly with the location of the photoisomerization. After a photoisomerization in the center of the disk, cGMP levels dropped dramatically in the overlying cytoplasm as a PDE was activated (Fig 2A). Over time, the decrement in cGMP spread radially, as cGMP diffused inward from the periphery and PDE*s on the disk surface diffused to increasing distances from the disk center. However, levels of cGMP near the plasma membrane never dropped very low, because of replenishment by longitudinal diffusion. In addition, CNG channel closure caused an initially local fall in $[Ca^{2+}]$ that stimulated cGMP synthesis by guanylate cyclase [1, 2], which was taken to be uniformly distributed on the disk membranes. This radial profile of cGMP is in general agreement with the previous results obtained with the fully space-resolved model [18, 20].

With a photoisomerization halfway between the center of the disk and the rim, the site of greatest cGMP depletion moved outward (Fig 2B). The change in cGMP at the nearest plasma membrane was greater, but followed a similar time course as before. A photoisomerization at the disk rim caused the largest and most rapid drop in cGMP at the plasma membrane near the site of photoisomerization (Fig 2C). But as cGMP levels began to recover there, cGMP fell to an even lower minimum in the interdiskal space halfway to the disk center. Later, as cGMP levels near the site of photoisomerization recovered further, the cGMP levels near the disk center continued to fall, dropping below the levels at the rim but never dropping below the levels halfway between the center and the rim.

The spatiotemporal profiles of cGMP in three dimensions within the outer segment, which were radially asymmetric except for the photoisomerization at the disk center (Fig 3A), were then used to compute the photocurrent responses. The two responses to rhodopsin photoisomerizations in the interior of the disk were similar but lagged that after a photoisomerization at the disk rim and were reduced in peak amplitude by nearly two-fold (Fig 4A). These differences in SPR amplitude and kinetics were more pronounced, but were otherwise in accordance with those reported previously [18]. In the present study, the steep, initial recovery in the SPR arising from a photoisomerization at the rim was caused by the greater local fall

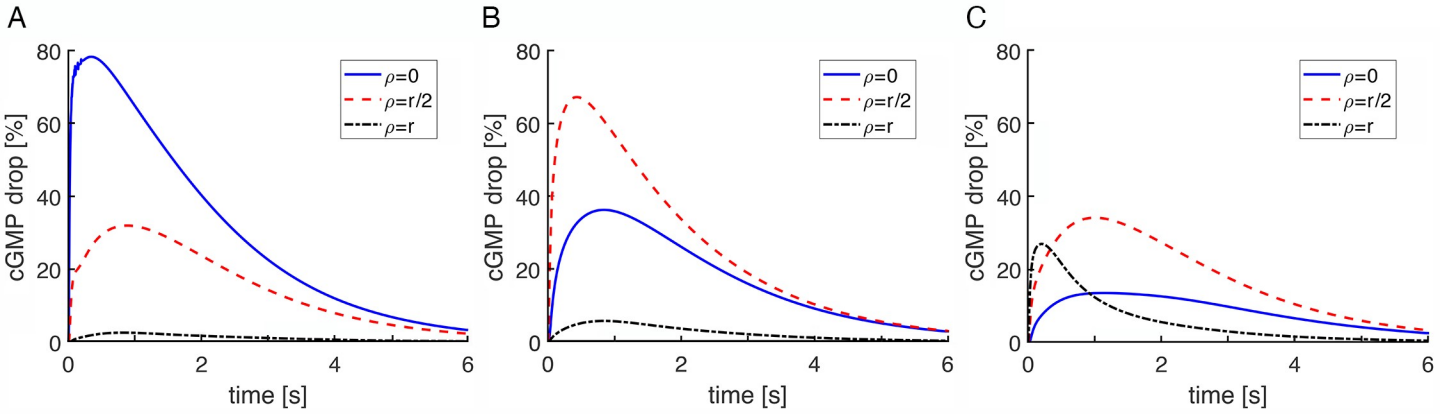

Fig 2. Dependence of spatiotemporal changes in cGMP on R* location in a salamander rod. At time zero, a photoisomerization was placed in the center of the disk (**A**), halfway between the center and the rim (**B**), or near the disk rim (**C**) in a rod lacking incisures. The relative drop in [cGMP] was computed at three interdiskal locations: next to the center of the activated disk (ρ = 0), halfway between the center of the disk and the disk rim (ρ = r/2), and near the disk rim (ρ = r). For (**A**), the changes in [cGMP] were radially symmetric, whereas for (**B** and **C**), the changes in [cGMP] at ρ = r/2 and ρ = r are shown only for the locations closest to the photoisomerization. Disk radius, r, was 5.5 μm and the diffusion coefficient for cGMP, D_{cG}, was 160 $\mu m^2/s$.

https://doi.org/10.1371/journal.pone.0240527.g002

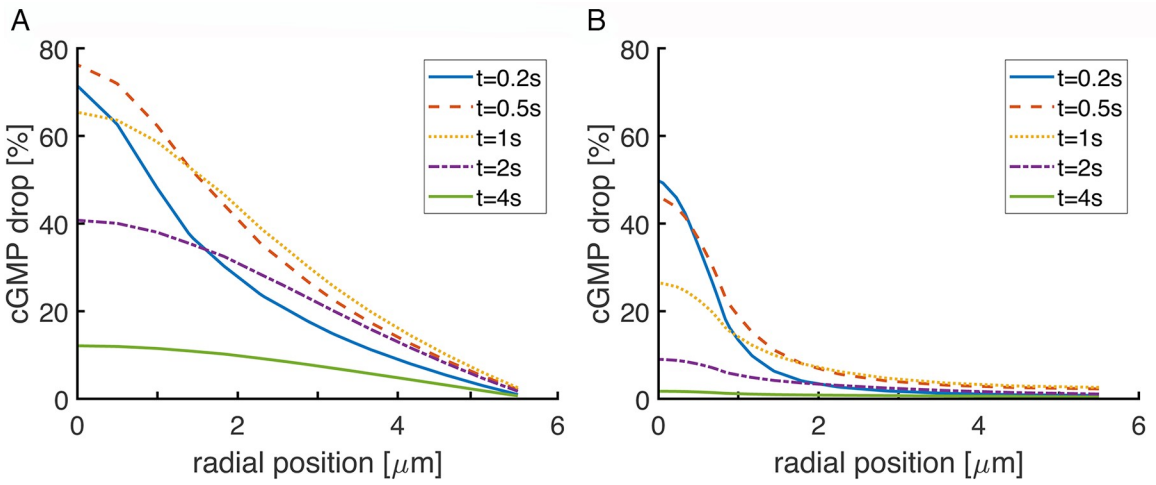

Fig 3. Reduced drop in cGMP and faster recovery with incisures in a salamander rod. The drop in cGMP is shown for the interdiskal space at the level of the active disk. The simulations were deterministic with the photoisomerization located in the center of the disk for a rod lacking incisures (**A**) and for a rod with 23 incisures evenly spread around the disk rim (**B**). Disk radius was 5.5 μm. Incisures extended 4.64 μm inward from the disk rim and were aligned in all disks.

https://doi.org/10.1371/journal.pone.0240527.g003

in Ca^{2+} and more powerful stimulation of guanylate cyclase near the plasma membrane. After ~ 2 s, guanylate cyclase activity was subsiding, but at axial distances several μm from the active disk, cGMP synthesis near the outer shell actually exceeded diffusion of cGMP towards the inactivating PDE^*s and cGMP levels climbed to levels higher than normally present in darkness. Eventually, rising Ca^{2+} levels inhibited this exuberant guanylate cyclase activity, and the presence of residual PDE^*s gave rise to a damped oscillation in the recovery phase. Differences in the SPRs were still present late in the recovery phase, eventually converging after about 3.5 s. These dramatic differences demonstrate that randomness in the R^* location contribute to variability over the early part of the SPR.

The relative contribution of R^* location to variability in the rising phase of the SPR was compared to the contribution of randomness in R^* phosphorylation by carrying out three sets of stochastic simulations. For set 1, R^* position was randomly chosen in each trial with an even distribution over the entire disk surface while R^* inactivated with a deterministic time course using average values for the duration of each phosphorylation state. For set 2, R^* position was fixed at the center of the disk, while the intervals between phosphorylation steps were chosen randomly from an exponential distribution with average equal to the average duration of each step. The average time for the first phosphorylation in the salamander rod was set to 83 ms, obtained by curve fitting of an experimental SPR (**S1 Fig** in S1 Appendix). R^* catalytic activity was decremented with the addition of each phosphate as described in [11, 19] (see **S2 Table** in S1 Appendix). For set 3, R^* location and phosphorylation of R^* were both randomized. One thousand simulations of total current, j_{tot}, were computed for each set of conditions. Variability was assessed as CV of the total current, the ratio of the standard deviation of j_{tot} to the mean of j_{tot}.

Randomness in R^* location dominated CV during the rising phase of the SPR (Fig 4B). For part of this period, CV was actually lower when R^* location and R^* shutoff were both randomized, indicating that by reducing R^* catalytic activity, early phosphorylations improved the reproducibility of the response to an R^* acting at different sites. Randomness in R^* shutoff became equally important near the peak of the SPR (Fig 4C) and superseded randomness in R^* location thereafter as the major source of variability throughout the recovery phase.

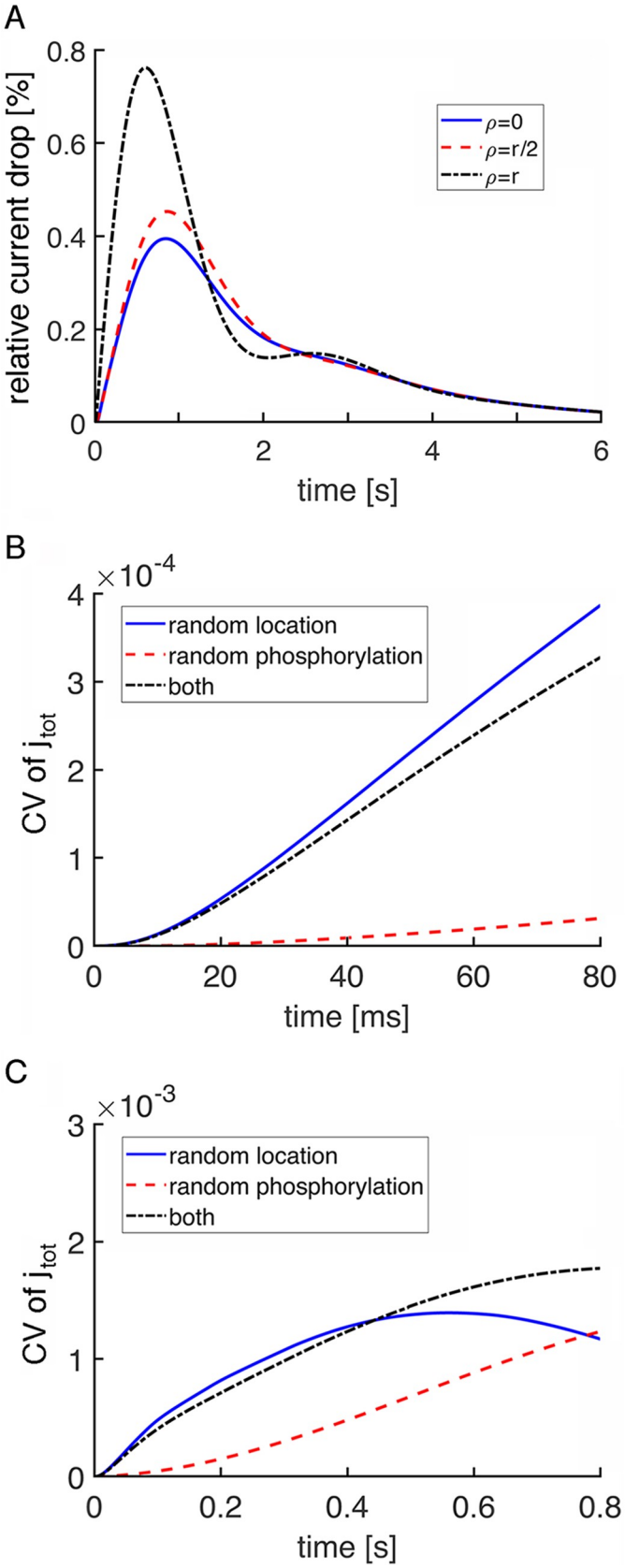

Fig 4. Larger, faster SPR elicited by R* at the disk rim of a salamander rod. (**A**) The three traces show %I(t) in a rod for R* positioned at: the disk center (ρ = 0), the disk rim (ρ = r), or an intermediate position (ρ = r/2), where r was

5.5 μm. The simulations were deterministic with the spread of transducin/PDE activation across the disk following the diffusion of heat on a surface and with R* and transducin/PDE activities shutting off over exponential time courses. The incisures were removed from all disks. (**B**) In stochastic simulations, randomness in R* location dominated CV of total current, $j_{tot}(t)$, at early times. (**C**) Later, towards the end of the rising phase of the SPR, CV due to randomness in R* location declined to match the CV due to randomness in R* shutoff.

https://doi.org/10.1371/journal.pone.0240527.g004

Incisures dampen the variability due to photoisomerization location

A salamander rod disk bears numerous incisures that penetrate deeply into its interior [8]. Given that incisures facilitate the axial diffusion of cGMP and Ca^{2+} in the aqueous cytosol, they enable a greater number of cGMP molecules to be hydrolyzed, spread the change in cGMP over a greater axial distance, and reduce the cGMP drop at the level of the activated disk (**Fig 3B**). Incisures also obstruct the diffusion of membrane proteins on the disk surface. Their influence over the SPR therefore affects both its amplitude and variability [18, 19]. The interaction of incisures with randomness in the location of photoisomerization was explored with deterministic simulations of the relative drop in current, %I(t) (**Fig 5A**), and with calculations of CV from stochastic simulations of total current, j_{tot} (**Fig 5B and 5C**) in salamander rods with 23 radial incisures arranged symmetrically in the disk. For the deterministic simulations, we considered five R* positions: center of the disk, halfway to the rim and midway between two incisures, halfway to the rim and adjacent to an incisure, at the rim and midway between two incisures, and at the rim and adjacent to an incisure.

The presence of incisures in the disk augmented the amplitudes of SPRs due to activations at all locations and reduced the amplitude difference between the response to activation at disk center and that at the disk rim from about 2-fold (**Fig 4A**) to less than 1.1-fold in deterministic simulations (**Fig 5A**). When the activation occurred next to an incisure, the drop in cGMP had a greater axial spread and the rate of change at the plasma membrane was slowed. As a result, the SPR was intermediate between that elicited by photoisomerization at disk center and that elicited at the rim between incisures, and became largely independent of radial R* location. The SPR was still largest for an activation at the rim, a result at variance with [18], where incisures caused a reversal so that the SPR became largest for an activation at the disk center. The basis was traced to the more rapid diffusion coefficient for PDE used in the earlier study; when the same value was adopted here, the reversal also occurred (results not shown). Greater access of PDE* to cGMP in the outer shell with incisures caused SPRs due to R*s at all locations on the disk to more closely resemble the response to an R* at the rim not only in size, but also in exhibiting the damped oscillation in the recovery phase.

Stochastic simulations revealed that incisures substantially decreased the CV due to randomness in R* location (**Fig 5B and 5C**) and had the opposite effect on CV due to randomness in R* phosphorylation. The former occurred because a symmetric pattern of long incisures tended to restrict the spread of activation to sectors of uniform size on the disk surface. The latter was caused by the incisures improving the axial diffusion of second messengers inside the rod and accordingly, reducing the local depletion of cGMP that would lower CV due to randomness in the rhodopsin phosphorylation, as described previously [18, 19]. There was also a more rapid decline in CV due to R* location such that CV due to R* phosphorylation matched it in importance at ~200 ms and far surpassed it by the peak of the SPR (**Fig 5C**).

A faster diffusion rate for cGMP within the outer segment supported larger SPRs with faster kinetics over the first ~4 s (**Fig 5D**). Slower diffusion of cGMP had the opposite effects. However, the SPRs produced by R*s in the disk center and at the disk rim were only marginally more similar in amplitude with the faster diffusion rate and the oscillation in the recovery became slightly more pronounced.

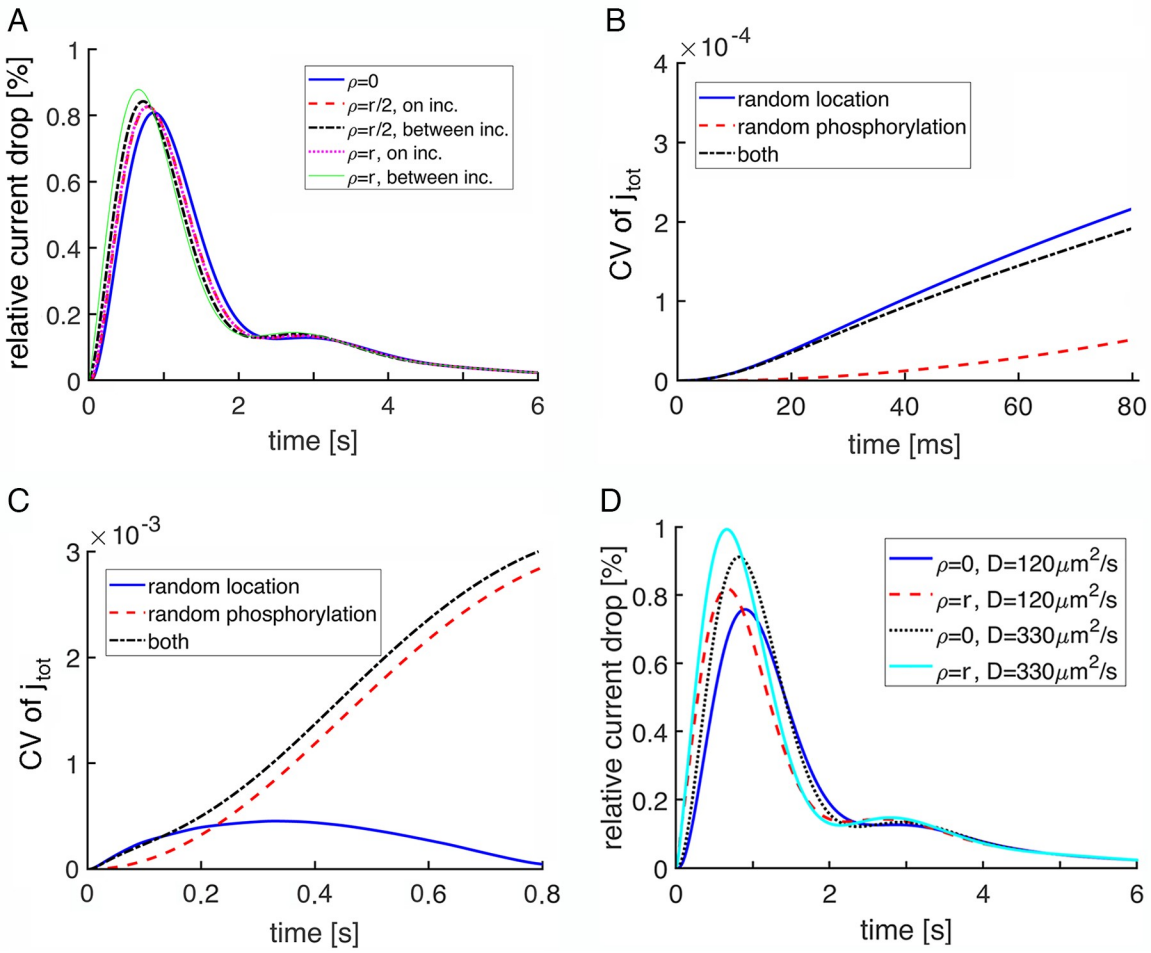

Fig 5. Early SPR variability reduced by multiple incisures in a salamander rod. Each disk had 23 incisures distributed evenly around its perimeter. Disk radius was 5.5 μm and each incisure extended 4.64 μm inward from the disk rim. Incisures were aligned in consecutive disks. (**A**) Deterministic simulations of %I(t) were computed for the R* located: at the disk center (ρ = 0), halfway to the rim (ρ = r/2) either midway between incisures or adjacent to one of them, and at the rim (ρ = r) either between incisures or adjacent to one of them. D_{cG} was 160 $\mu m^2/s$. (**B**) CV for j_{tot} was dominated by randomness in R* location during the initial rising phase of the SPR, based on stochastic simulations. R* was located in the middle of the disk for trials with random R* phosphorylation. (**C**) CV due to randomness in R* location subsided over time and was eventually surpassed by CV due to randomness in R* phosphorylation at ~0.25 time to the peak of the SPR. (**D**) Deterministic simulations comparing the %I(t) after a photoisomerization at the disk center or at the rim halfway between two adjacent incisures for two different D_{cG} values.

https://doi.org/10.1371/journal.pone.0240527.g005

Negligible effects of activation location in mouse rods

It can be expected that SPR variability due to randomness in the position of photoisomerization should disappear with decreasing disk size. Mouse rod disks have a radius that is ~1/10th that of the largest salamander rod disks. Nevertheless, a photoisomerization at the center of the disk produced a radial gradient in cGMP within the interdiskal space (Fig 6A). Inhomogeneities in cGMP levels would diminish and dissipate faster if cGMP were to diffuse very rapidly. Ranges of values have been reported for the axial diffusion of cGMP and for the tortuosity factor in the rod [36–39], so gradients were calculated for two diffusion coefficient values for cGMP that differed by 2.75-fold. The local drop in cGMP was greater with the lower diffusion coefficient, but clear gradients were formed in both cases.

As expected, rhodopsin activation position had a much smaller effect on SPR variability in mouse because all locations on the disk were proximal to the CNG channels in the plasma

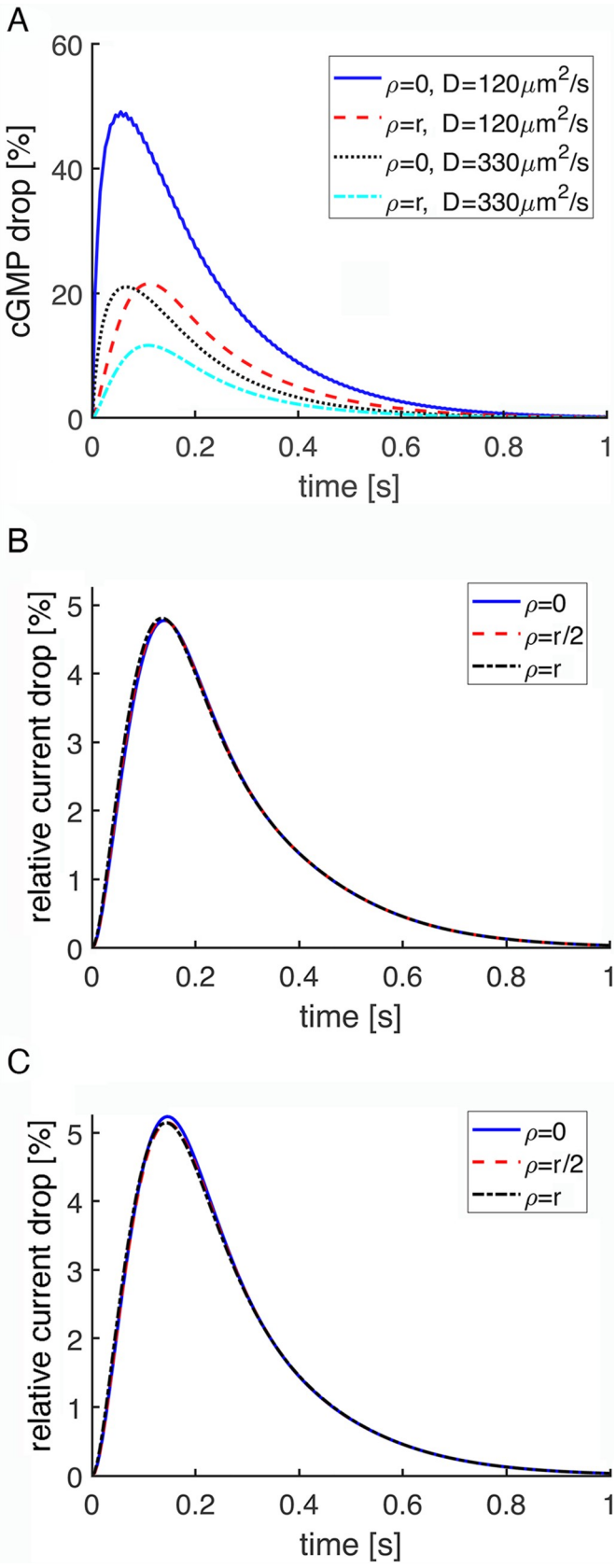
A
cGMP drop [%]
time [s]
ρ=0, D=120μm²/s
ρ=r, D=120μm²/s
ρ=0, D=330μm²/s
ρ=r, D=330μm²/s
B
relative current drop [%]
time [s]
ρ=0
ρ=r/2
ρ=r
C
relative current drop [%]
time [s]
ρ=0
ρ=r/2
ρ=r

Fig 6. Low SPR variability due to R* position in a mouse rod despite radial gradients of cGMP. (**A**) Gradients were computed for an R* in the center of the disk for disks lacking an incisure using two different values for the diffusion coefficient of cGMP. Disk radius, r, was 0.685 μm. (**B**) Variability in SPR due to R* location was low for disks lacking the incisure. R* was placed at the disk center (ρ = 0), halfway to the rim (ρ = r/2), or at the rim (ρ = r). (**C**) The SPR was larger and variability increased, when each disk had a single incisure. The incisure penetrated radially 0.31 μm into the disk interior. Incisures were aligned in disks throughout the outer segment. D_{cG} was 120 $\mu m^2 s^{-1}$ for simulations in (**B**) and (**C**).

https://doi.org/10.1371/journal.pone.0240527.g006

membrane. In deterministic runs, the SPR changed very little with R* location in the absence of the incisure (Fig 6B). The incisure increased SPR amplitudes somewhat (Fig 6C), by facilitating the axial diffusion of cGMP within the outer segment after hydrolysis at the activated disk, consistent with previous findings [24], but made the disparity between SPRs arising from photoisomerizations at the different disk locations slightly greater.

In contrast to the salamander rod SPR, a damped oscillation was not present late in the recovery of the mouse rod SPR either with or without the incisure and irrespective of R* location (Fig 6B and 6C). Even though the drop in cGMP was greater in mouse rods compared to that in salamander rods, the timing of events was different. In salamander rods, the return of guanylate cyclase activity towards its basal level in darkness was met with a residual PDE* activity that effected a small, secondary drop in circulating current. But in mouse rods, PDE* inactivation was already complete by the time guanylate cyclase activity recovered to its basal level in darkness, so the damped oscillation did not occur.

Stochastic SPR simulations indicated that CV for j_{tot} in mouse was dominated by randomness in R* phosphorylation except for a very early segment of the rising phase (Fig 7). Mouse rod SPRs were experimentally shown to have faster kinetics than those of salamander rods [40, 41], as reflected in **S1** and **S2 Figs** in S1 Appendix, and in mouse rod simulations with stochastic R* shutoff, the average time taken for the first phosphorylation was 16 ms [11]. There were three main differences from salamander with respect to variability. First, the switch to the randomness of R* phosphorylation prevailing as the main contributor of variability occurred at ~7 ms in mouse (Fig 7A and 7B), much sooner than at 800 ms in salamander rods lacking incisures (Fig 4C) and at 220 ms in salamander rods with incisures (Fig 5C), due to the faster equilibration of cGMP within the smaller cytosolic volume between disks and faster phosphorylation of R* in mouse. Second, randomness in R* location contributed a negligible amount of variability in mouse even during the rising phase. Third, the presence of a single incisure in each mouse disk had the opposite effect on CV (Fig 6B and 6C) than the presence of multiple, symmetrically placed incisures in each salamander disk (**Figs 4 and 5**). In mouse, CV due to randomness in R* location was quite a bit higher with the incisure because it introduced spatial asymmetry to the disk surface, i.e., a diffusion barrier for R*, activated transducin, and PDE* (Fig 7C and 7D). The high CV of j_{tot} from both sources at the peak of the SPR in mouse rods, compared to that in salamander rods, has a trivial origin, arising from the smaller circulating current in mouse. As will be shown below, that difference is minimal in more informative comparisons of CV of the relative current drop (Fig 10).

Dependence of variability on disk radius

Differences in the contribution of photoisomerization position to SPR variability between small mouse rods and large salamander rods were consistent with a dependence upon disk size. But the time course of the SPR is considerably faster in mouse than in salamander and many key phototransduction parameters vary between mouse and salamander, so the effect of geometry alone was explored by varying disk size in an idealized rod that had the physical and kinetic parameters of a salamander rod except for the removal of all incisures. Disk radius was

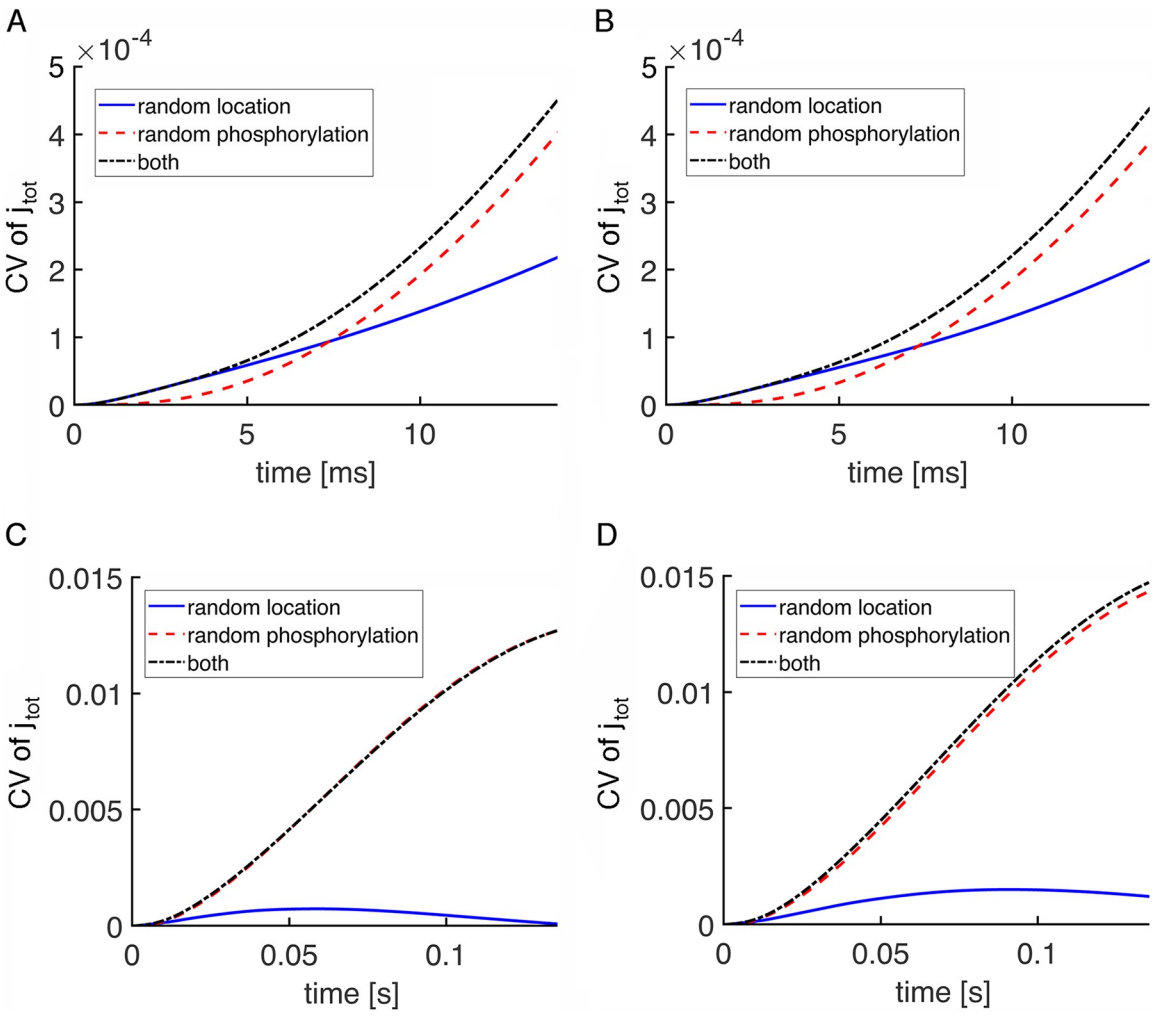

Fig 7. CV of the total current due to two sources of variability in a mouse SPR. Randomness in the shutoff of R* dominated CV of the total current, $j_{tot}(t)$, over most of the duration of the SPR. The exception was at very early times after photon absorption, when randomness in the location of the photoisomerization contributed more variability as shown on an expanded time scale (**A, B**). The incisure was absent in simulations in (**A, C**) and was present for simulations in (**B, D**). D_{cG} was 120 $\mu m^2 s^{-1}$.

https://doi.org/10.1371/journal.pone.0240527.g007

systematically reduced from 6 μm to 1 μm, keeping constant the ionic channel density on the outer shell among the various cases. Stochastic simulations were computed by letting in each trial, the photoisomerization location be randomly chosen on the midstack disk. For reference, rod outer segment radius is 0.7 μm in mouse [5], 2.5–3 μm in toad [42] and up to 6.5 μm in salamander [6–8].

Variability did not decrease systematically with diminution of radius, based on calculations of the CV of the total current (**Fig 8A**). The reason is that the results were confounded by having held constant the ionic channel density in the outer shell for all disk radii, which resulted in a decrease in circulating current with smaller radii. In computing the CV of the total current, the mean current appearing in the denominator was very large, essentially equal to the dark current, so the relatively small decreases in the standard deviation of the change in total current in large rods were offset by corresponding decreases in the circulating current. This interpretation was confirmed with plots of the standard deviation of the total current, which showed that the total current was clearly more variable in cases of larger radii (**Fig 8B**). It was

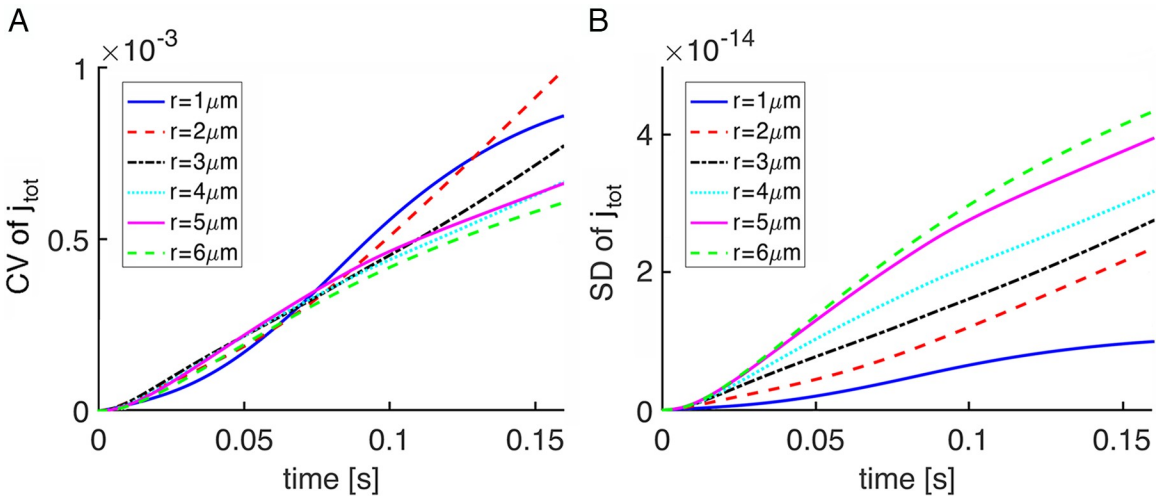

Fig 8. Variability in SPR total current due to R* location in salamander rods of decreasing size. (**A**) Early SPR variability due to randomness in R* location changed very little with decreasing disk radii, when assessed by CV of the total current, $j_{tot}(t)$. (**B**) In contrast, the standard deviation of the total current decreased systematically with a reduction in disk radius. Disks lacked incisures.

https://doi.org/10.1371/journal.pone.0240527.g008

therefore more instructive to express variability in terms of CV of the relative current drop, I (t) (Fig 9), in order to reveal the systematic decrease in variability with reduction in disk radius. During the first few ms, CV was very high for rods of all sizes due to the very small amplitude of the SPR. CV would not be biologically meaningful during this time because the response would not yet have risen out of the continuous noise of the phototransduction cascade. With small rods, CV fell to low levels rather quickly, but several hundred ms were needed for that to happen in the largest rods.

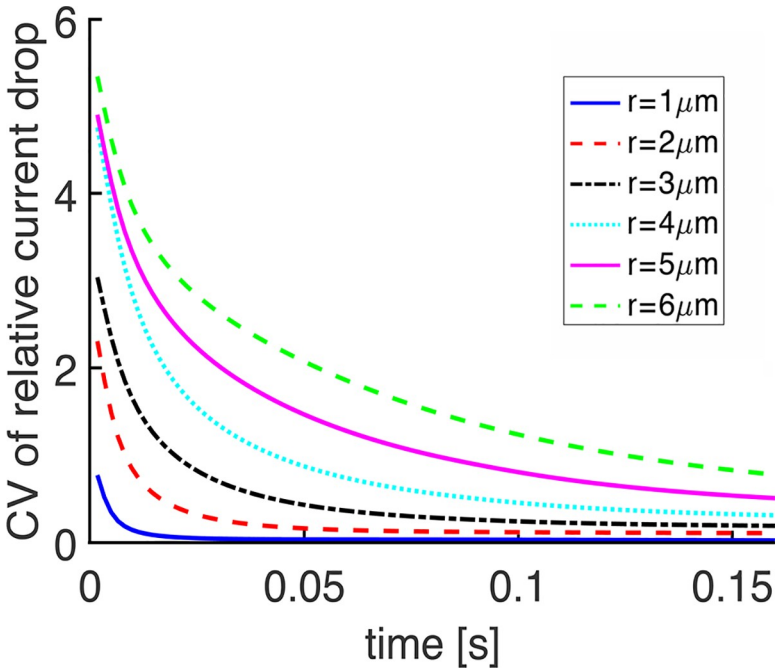

Fig 9. Systematic decrease in CV of I(t) with reduction in disk radius in salamander rods. R* location on the disk was chosen randomly in each trial and R* and PDE* activities declined exponentially over time. Disks lacked incisures.

https://doi.org/10.1371/journal.pone.0240527.g009

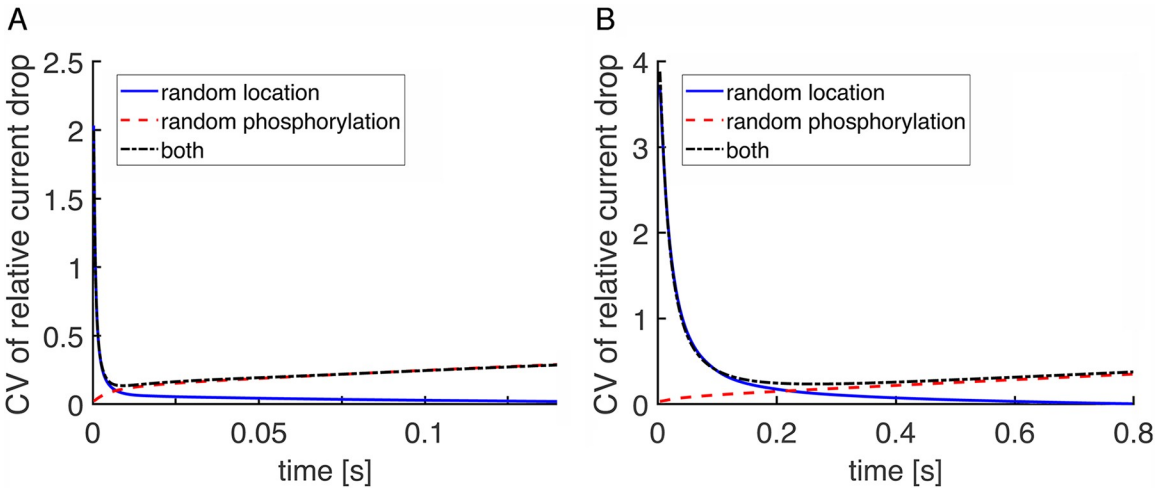

Fig 10. Lower initial CV of I(t) and faster decline in wild type mouse and salamander rods. CV of the relative drop in current, I(t), is plotted over time just beyond the SPR time to peak in: (**A**) a mouse rod with disk radius = 0.685 μm and one incisure and (**B**) a salamander rod with disk radius = 5.5 μm and 23 incisures.

https://doi.org/10.1371/journal.pone.0240527.g010

Finally, CV of the relative drop in current, I(t), is reported, comparing results for wild type mouse (Fig 10A) and large, wild type salamander (Fig 10B) rods with incisures. The behavior of the curves led to similar conclusions for the role of the randomness in the photoisomerization site and for the role of the incisures. Notice that the curves of CV due to randomness in the activation site began with a peak. This was because the amplitude of the relative drop in current at early times was very small, yielding large CV values even for a modest standard deviation. The CV generated by both factors was higher in salamander than in mouse, consistent with results of [19], but in apparent contradiction to the results shown for the total current CV (**Figs** 5 and 7). As a matter of fact, this was only due to the mean of the total current during the SPR being close to the dark current value, which was larger in salamander than in mouse. When the relative drop in current was analyzed, the dark current was normalized, so it did not influence the CV.

In mouse, CV for the relative current drop due to randomness in the location of photoisomerization fell to ~0.09 after 7 ms, when randomness in R^* phosphorylation became the dominant source of variability. In salamander, CV due to random location of photoisomerization was ~0.4 after 100 ms and was still ~0.2 after 200 ms. Thereafter, randomness in R^* phosphorylation became the dominant source of variability. Hence variability due to randomness in photoisomerization location was insignificant at the peak of the salamander SPR, where CV due to randomness in R^* phosphorylation was about 0.35. Experimental determinations of CV are not yet available for salamander rods, but for toad rods, that tend to have a disk radius of ~3 μm, CV at the peak of the SPR due to all sources is ~0.2 [27] and for mouse rods it is ~0.3 [43].

In conclusion, these simulations indicated that the rising phase of the SPR generated by a salamander rod with a large cross section was more prone to variability due to randomness in the location of rhodopsin photoisomerization than rods with a small cross section, such as those of mouse, which closely resemble human rods. Incisures mitigated this source of variability by reducing the magnitude and shortening the time course over which it exerted its effect in salamander. Interestingly, the single incisure in mouse disks had the opposite effect on variability due to photoisomerization location because it created a non-symmetric condition, but the overall variability remained too small to impact signaling.

Discussion

The capacity for rhodopsin to form dimers and higher order oligomers raises questions about its mobility in the disk membrane. The lateral diffusion of rhodopsin has been measured many times in amphibian rods in the last 40 years. Early measurements of unmodified rhodopsin [26, 44], as well as rhodopsin labeled with rhodamine [45], yielded coefficients of 3–5 x 10^{-9} cm^2 s^{-1}. Rapid rotational diffusion was also consistent with a single rhodopsin molecule moving within the disk membrane. Later it became accepted that early measurements, at least those that used unmodified rhodopsin, were partially compromised by the emergence of metarhodopsin III so these measurements were performed again and yielded a more complex picture [46]. The lipid environment of disk membranes in Xenopus was shown to be non-homogeneous, with apparent lipid rafts, which could be destroyed by using cholesterol-depleting drugs [47]. In the dark and immediately after photoexcitation both rhodopsin-EGFP and EGFP-tagged transducin diffuse freely in the bulk of fluid lipid. Slowing of diffusion was observed upon the formation of the complex of R^* with transducin [47]. Cholesterol depletion prevented this slowing, suggesting that these complexes either move to less fluid microdomains, or induce the formation of cholesterol-containing membrane microdomains around them. The more recent measurement was performed with unmodified rhodopsin in amphibian (frog, toad, and salamander) and gecko rods [46]. In all cases, after elimination of the metarhodopsin III contribution, rhodopsin diffusion was found to be essentially the same as previously reported, with a diffusion coefficient of 5×10^{-9} cm^2 s^{-1}. Yet the authors found that a fraction of the rhodopsin, which varied from virtually zero to 100%, was immobile. The authors were unable to establish the factor(s) that determined the size of this fraction. This immobile fraction might represent paracrystalline rhodopsin structures reported in disks immobilized on mica [48]. Govardovskii et al. [46] hypothesized that the fraction of immobile rhodopsin might be controlled physiologically to regulate the sensitivity of the phototransduction cascade, implying that only freely mobile rhodopsin mediates signaling. This is consistent with the demonstration that monomeric rhodopsin is necessary and sufficient to activate transducin [49, 50], become phosphorylated by GRKs [51, 52] and bind arrestin [51–53]. It was also established that arrestin binds rhodopsin at 1:1 ratio, both in vitro [51, 54] and in mouse photoreceptors [55]. The functional findings were further validated by the elucidation of structures of rhodopsin complexes with G protein [56], GRKs [57], and arrestin [58, 59]. At the moment, there is no evidence for the participation of anything greater than a single molecule of light-activated rhodopsin in visual signaling. Indeed, it was established long ago that rods respond to single photons [27], which can activate only one molecule of rhodopsin. Based on available information, we modeled visual signal transduction assuming free diffusion of monomeric rhodopsin within the disk membrane. In the future, it would be interesting to explore with the model, how rhodopsin dimers and higher order oligomers of immobile multi-rhodopsin formations impact cascade dynamics and the spatial distribution of cGMP over the duration of the SPR.

By assuming that radial cGMP gradients in the interdiskal space equilibrate with infinite rapidity relative to the time course of the SPR, globally well stirred and transversely well stirred models of visual transduction disregard any possibility that the transverse position of rhodopsin photoisomerization on the disk could produce variability in the SPR. The fully space-resolved model invalidated that assumption in hypothetical salamander rods lacking incisures by showing that transverse gradients of cGMP concentration were created by a photoisomerization [18, 20], that the gradients evolved over a time scale of seconds, and that the form of the gradient depended upon the radial location of the photoisomerization on the disk (**Fig 2**). Salamander disks are large, with a radius of 5.5 μm, but mouse rod disks have a radius that is

8-fold smaller, enabling cGMP gradients in the interdiskal space to dissipate more rapidly. Nevertheless, marked radial gradients in cGMP were still present late into the time course of the SPR of hypothetical mouse rods lacking incisures (Fig 6A). Increasing the diffusion of cGMP by nearly 3-fold reduced the magnitude of the drop in cGMP, but did little towards changing the difference in the drop in cGMP levels in the center of the disk relative to that at the rim, for a centrally located photoisomerization.

Our modeling allowed subunits of the PDE dimer to be activated individually by single GTP-bound transducin molecules (see Methods and S1 Appendix). However, a recent study found that in the presence of membrane, i.e., under native conditions, a single transducin bound to the PDE dimer produced little if any increase in hydrolytic activity [25]. PDE activation required the binding of two transducins. To test whether the requirement for two transducins to activate PDE would change our conclusions, some simulations were performed by incorporating this feature into our model. The results are shown in S1 File. The radial cGMP gradients produced by an R* located in the center of a mouse disk were not substantially altered (**S4 Fig**) nor were there any significant effects on CV during the rising phase of the SPR (**S5 Fig**).

Although the radial cGMP gradients gave rise to fairly minor differences in SPR kinetics and amplitudes in mouse rods (Fig 6B and 6C), the differences were sizeable in salamander rods (Fig 4A; see also **Fig 7B** in [18]). The basis for the disparity across species was explored by systematically varying disk radius (**Figs 8 and 9**). Larger disk size generated increasing variability in the rising phase of the SPR. The reason is that due to the finite diffusion rate of cGMP, longer time periods would pass between the initial, local depletion of cGMP near the photoactivation site on the disk and the reduction of cGMP at the plasma membrane, where it would lead to closure of the CNG channels. These results confirm the hypothesis that the initially high CV followed by a decline during the early rising phase of the SPR was due to randomness in the site of photoisomerization on the disk [19].

Our approach may have overestimated CV due to phosphorylation at early times because in our simulations, phosphorylation of R* began to decrease its activity within a few tens of ms after photoisomerization, whereas experimental evidence indicates that it occurs just before the peak of the SPR in mouse rods [16, 17]. The small contribution of the random rate of transducin/PDE activation to overall variability was omitted because that part of the cascade was deterministic in our simulations.

In our treatment, basal PDE activity was taken to be uniform over time and space, but in reality, it arises from spontaneous activations of PDE molecules that occur throughout the rod and generate "continuous noise" [60]. The inhomogeneity in cGMP levels over time and space caused by random PDE activations adds further variability to the early, rising phase of the SPR. It was removed in our analysis in order to isolate the contribution of photoisomerization location to variability. However, as the response to R* grows, the impact of both sources of variability diminishes as more PDE*s are recruited across the disk surface and the depletion of cGMP spreads over a greater volume.

In small diameter mouse rods, the presence of a single incisure increased the size of the SPR and enhanced its variability slightly, by allowing cGMP gradients to dissipate axially and by distorting the spread of transducin/PDE activation across the disk surface (Fig 6B and 6C). However, variability due to R* location was never very large in mouse rods even in the presence of an incisure and it faded after the first 100 ms (Fig 7). Thus, it appears that the biological role of a single incisure in relatively small disks, such as those in mouse, is not to improve SPR reproducibility.

In contrast, SPR variability was reduced by multiple incisures arranged symmetrically around the disk perimeter in salamander rods (**Figs 4** vs **5**). Nevertheless, CV of the relative current drop was still quite high in salamander rods for the first hundred ms (Fig 10B),

consistent with [19]. The incisures acted in two ways. By cordoning off wedge shaped sections of the disk, they caused R* to activate a more uniform compartment of the disk membrane surface [19]. In addition, due to faster axial diffusion, they reduced the drop in cGMP concentration near the activated disk and spread the change over a greater length of the outer segment. The conclusion that SPRs arising from photoisomerizations in the center of the disk and at the rim would be similar in large amphibian rods with incisures as well as in small mouse rods is supported by electrophysiological recordings of single toad rods [28]. Stimulation of the rod with a narrow slit of light passing through the full diameter of its outer segment gave rise to dim flash responses that were similar in form to those with the slit placed on the edge of the outer segment. Variability for the SPRs elicited at the two slit positions was not analyzed, so the predicted difference in CV in the initial segment of the rising phase awaits confirmation. Another experimental prediction is that CV in the early rising phase of the SPR would be greater in large amphibian rods lacking incisures. This prediction is more difficult to test because thus far, rods with large disks lacking incisures have not been found in nature. Interestingly, disks in human rods are only slightly larger than those of mouse, yet form a more symmetric pattern of multiple, shallow incisures [61].

The slow time course of the rod response, which is necessary for amplification, impedes temporal resolution. To improve upon signaling of photon arrival while suppressing the high frequency continuous noise generated by the phototransduction cascade in the rod, rod signals undergo band pass filtering at the bipolar cell [4, 62]. Thus, bipolar cells "pay particular attention" to the rising phase of the SPR, which makes the variability during this period more important biologically. Variability in the rising phase of the SPR subsides quickly in small diameter mouse rods, but is more substantial and protracted in large salamander rods. A less "reliable" rising phase may explain why the rod bipolar cell response to the SPR of the rod appears to be accelerated less in salamander than in mouse [3, 4, 63]. This variability must impose a more severe limitation on the speed of salamander rod vision based on the SPRs of single rods.

Rod bipolar cells receive convergent input from 10–25 rods in salamander and in mouse [64–66]. Considering a greater than 4-fold amplification of the rod signal in the rod bipolar cell [3, 67–69], summation of the phototransduction cascade noise from all of these rods would make single photon detection impossible. As a countermeasure, rod bipolar cells perform a thresholding operation [69–71]. Release of glutamate neurotransmitter at the rod to rod bipolar cell synapse is saturating, rendering the small reductions in release due to continuous noise insufficient to elicit a postsynaptic response. Thresholding also causes the rod bipolar cell to ignore the very initial segment of the rising phase of the rod SPR, the period of greatest variability due to randomness in R* location. Thus, in addition to intra-rod mechanisms, e.g., [22], thresholding by bipolar cells contributes to the accuracy of photon counting by the visual system in dim light.

Supporting information

S1 Appendix. Fully space-resolved model and parameter sets.
(PDF)

S1 File. Simulations in which two transducins are necessary for PDE activation.
(PDF)

Author Contributions

Investigation: Giovanni Caruso, Colin J. Klaus, Heidi E. Hamm, Vsevolod V. Gurevich, Clint L. Makino, Emmanuele DiBenedetto.

Writing – original draft: Giovanni Caruso, Colin J. Klaus, Heidi E. Hamm, Vsevolod V. Gurevich, Clint L. Makino, Emmanuele DiBenedetto.

Writing – review & editing: Giovanni Caruso, Colin J. Klaus, Heidi E. Hamm, Vsevolod V. Gurevich, Clint L. Makino, Emmanuele DiBenedetto.

References

1. Ingram NT, Sampath AP, Fain GL. Why are rods more sensitive than cones? J Physiol (Lond). 2016; 594: 5415–5426.
2. Vinberg F, Chen J, Kefalov VJ. Regulation of calcium homeostasis in the outer segments of rod and cone photoreceptors. Prog Ret Eye Res. 2018; 67: 87–101.
3. Field GD, Rieke F. Nonlinear signal transfer from mouse rods to bipolar cells and implications for visual sensitivity. Neuron. 2002; 34: 773–785. https://doi.org/10.1016/s0896-6273(02)00700-6 PMID: 12062023
4. Armstrong-Gold CE, Rieke F. Bandpass filtering at the rod to second-order cell synapse in salamander (*Ambystoma tigrinum*) retina. J Neurosci. 2003; 23: 3796–3806. https://doi.org/10.1523/JNEUROSCI.23-09-03796.2003 PMID: 12736350
5. Carter-Dawson LD, LaVail MM. Rods and cones in the mouse retina. I. Structural analysis using light and electron microscopy. J Comp Neurol. 1979; 188: 245–262. https://doi.org/10.1002/cne.901880204 PMID: 500858
6. Hárosi FI. Absorption spectra and linear dichroism of some amphibian photoreceptors. J Gen Physiol. 1975; 66: 357–382. https://doi.org/10.1085/jgp.66.3.357 PMID: 808586
7. Chen Y, Znoiko S, DeGrip WJ, Crouch RK, Ma JX. Salamander blue-sensitive cones lost during metamorphosis. Photochem Photobiol. 2008; 84: 855–862. https://doi.org/10.1111/j.1751-1097.2008.00310.x PMID: 18331398
8. Mariani AP. Photoreceptors of the larval tiger salamander retina. Proc Roy Soc Lond B Biol Sci. 1986; 227: 483–492.
9. Rieke F, Baylor DA. Origin of reproducibility in the responses of retinal rods to single photons. Biophys J. 1998; 75: 1836–1857. https://doi.org/10.1016/S0006-3495(98)77625-8 PMID: 9746525
10. Whitlock GG, Lamb TD. Variability in the time course of single photon responses from toad rods: termination of rhodopsin's activity. Neuron. 1999; 23: 337–351. https://doi.org/10.1016/s0896-6273(00)80784-9 PMID: 10399939
11. Caruso G, Bisegna P, Lenoci L, Andreucci D, Gurevich VV, Hamm HE, et al. Kinetics of rhodopsin deactivation and its role in regulating recovery and reproducibility of rod photoresponse. PLoS Comput Biol. 2010; 6: e1001031. https://doi.org/10.1371/journal.pcbi.1001031 PMID: 21200415
12. Vishnivetskiy SA, Raman D, Wei J, Kennedy MJ, Hurley JB, Gurevich VV. Regulation of arrestin binding by rhodopsin phosphorylation level. J Biol Chem. 2007; 282: 32075–32083. https://doi.org/10.1074/jbc.M706057200 PMID: 17848565
13. Arshavsky VY, Dizhoor AM, Shestakova IK, Philippov P. The effect of rhodopsin phosphorylation on the light-dependent activation of phosphodiesterase from bovine rod outer segments. FEBS Lett. 1985; 181: 264–266. https://doi.org/10.1016/0014-5793(85)80272-6 PMID: 2982661
14. Miller JL, Fox DA, Litman BJ. Amplification of phosphodiesterase activation is greatly reduced by rhodopsin phosphorylation. Biochemistry. 1986; 25: 4983–4988. https://doi.org/10.1021/bi00366a002 PMID: 3021208
15. Xu J, Dodd RL, Makino CL, Simon MI, Baylor DA, Chen J. Prolonged photoresponses in transgenic mouse rods lacking arrestin. Nature. 1997; 389: 505–509. https://doi.org/10.1038/39068 PMID: 9333241
16. Chen J, Makino CL, Peachey NS, Baylor DA, Simon MI. Mechanisms of rhodopsin inactivation in vivo as revealed by a COOH-terminal truncation mutant. Science. 1995; 267: 374–377. https://doi.org/10.1126/science.7824934 PMID: 7824934
17. Chen CK, Burns ME, Spencer M, Niemi GA, Chen J, Hurley JB, et al. Abnormal photoresponses and light-induced apoptosis in rods lacking rhodopsin kinase. Proc Natl Acad Sci USA. 1999; 96: 3718–3722. https://doi.org/10.1073/pnas.96.7.3718 PMID: 10097103
18. Caruso G, Bisegna P, Shen L, Andreucci D, Hamm HE, DiBenedetto E. Modeling the role of incisures in vertebrate phototransduction. Biophys J. 2006; 91: 1192–1212. https://doi.org/10.1529/biophysj.106.083618 PMID: 16714347

19. Bisegna P, Caruso G, Andreucci D, Shen L, Gurevich VV, Hamm HE, et al. Diffusion of the second messengers in the cytoplasm acts as a variability suppressor of the single photon response in vertebrate phototransduction. Biophys J. 2008; 94: 3363–3383. https://doi.org/10.1529/biophysj.107.114058 PMID: 18400950

20. Caruso G, Gurevich VV, Klaus C, Hamm H, Makino CL, DiBenedetto E. Local, nonlinear effects of cGMP and Ca^{2+} reduce single photon response variability in retinal rods. PLoS ONE. 2019; 14: e0225948. https://doi.org/10.1371/journal.pone.0225948 PMID: 31805112

21. Cohen AI. The ultrastructure of the rods of the mouse retina. Am J Anat. 1960; 107: 23–48. https://doi.org/10.1002/aja.1001070103 PMID: 13694328

22. Caruso G, Bisegna P, Andreucci D, Lenoci L, Gurevich VV, Hamm HE, et al. Identification of key factors that reduce the variability of the single photon response. Proc Natl Acad Sci USA. 2011; 108: 7804–7807. https://doi.org/10.1073/pnas.1018960108 PMID: 21518901

23. Andreucci D, Bisegna P, Caruso G, Hamm HE, DiBenedetto E. Mathematical model of the spatio-temporal dynamics of second messengers in visual transduction. Biophys J. 2003; 85:1358–1376. https://doi.org/10.1016/S0006-3495(03)74570-6 PMID: 12944255

24. Shen L, Caruso G, Bisegna P, Andreucci D, Gurevich VV, Hamm HE, et al. Dynamics of mouse rod phototransduction and its sensitivity to variation of key parameters. IET Syst Biol. 2010; 4: 12–32. https://doi.org/10.1049/iet-syb.2008.0154 PMID: 20001089

25. Qureshi BM, Behrmann E, Schöneberg J, Loerke J, Bürger J, Mielke T, et al. It takes two transducins to activate the cGMP-phosphodiesterase 6 in retinal rods. Open Biol. 2018; 8: 180075. https://doi.org/10.1098/rsob.180075 PMID: 30068566

26. Poo M, Cone RA. Lateral diffusion of rhodopsin in the photoreceptor membrane. Nature. 1974; 247: 438–441. https://doi.org/10.1038/247438a0 PMID: 4818543

27. Baylor DA, Lamb TD, Yau KW. Responses of retinal rods to single photons. J Physiol (Lond). 1979; 288: 613–634.

28. Lamb TD, McNaughton PA, Yau KW. Spatial spread of activation and background desensitization in toad rod outer segments. J Physiol (Lond). 1981; 319: 463–496.

29. Schnapf JL. Dependence of the single photon response on longitudinal position of absorption in toad rod outer segments. J Physiol (Lond). 1983; 343: 147–159.

30. Mazzolini M, Facchetti G, Andolfi L, Proietti Zaccaria R, Tuccio S, Treu J, et al. The phototransduction machinery in the rod outer segment has a strong efficacy gradient. Proc Natl Acad Sci USA. 2015; 112: E2715–E2724. https://doi.org/10.1073/pnas.1423162112 PMID: 25941368

31. Yau KW, Baylor DA. Cyclic GMP-activated conductance of retinal photoreceptor cells. Annu Rev Neurosci. 1989; 12: 289–327. https://doi.org/10.1146/annurev.ne.12.030189.001445 PMID: 2467600

32. Baylor DA, Lamb TD, Yau KW. The membrane current of single rod outer segments. J Physiol (Lond). 1979; 288: 589–611.

33. Reingruber J, Pahlberg J, Woodruff ML, Sampath AP, Fain GL, Holcman D. Detection of single photons by toad and mouse rods. Proc Natl Acad Sci USA. 2013; 110: 19378–19383. https://doi.org/10.1073/pnas.1314030110 PMID: 24214653

34. Yamada E. The fine structure of retina studied with electron microscope. I. The fine structure of frog retina. Kurume Med J. 1957; 4: 127–147.

35. Fernández-Morán H. Fine structure of biological lamellar systems. Rev Mod Phys. 1959; 31: 319–330.

36. Olson A, Pugh EN Jr. Diffusion coefficient of cyclic GMP in salamander rod outer segments estimated with two fluorescent probes. Biophys J. 1993; 65: 1335–1352. https://doi.org/10.1016/S0006-3495(93)81177-9 PMID: 8241412

37. Koutalos Y, Nakatani K, Yau KW. Cyclic GMP diffusion coefficient in rod photoreceptor outer segments. Biophys J. 1995; 68: 373–382. https://doi.org/10.1016/S0006-3495(95)80198-0 PMID: 7536055

38. Koutalos Y, Brown RL, Karpen JW, Yau KW. Diffusion coefficient of the cyclic GMP analog 8-(fluoresceinyl)thioguanosine 3', 5' cyclic monophosphate in the salamander rod outer segment. Biophys J. 1995; 69: 2163–2167. https://doi.org/10.1016/S0006-3495(95)80090-1 PMID: 8580360

39. Holcman D, Korenbrot JI. Longitudinal diffusion in retinal rod and cone outer segment cytoplasm: the consequence of cell structure. Biophys J. 2004; 86: 2566–2582. https://doi.org/10.1016/S0006-3495(04)74312-X PMID: 15041693

40. Bader CR, Macleish PR, Schwartz EA. A voltage-clamp study of the light response in solitary rods of the tiger salamander. J Physiol (Lond). 1979; 296: 1–26.

41. Raport CJ, Lem J, Makino C, Chen CK, Fitch CL, Hobson A, et al. Downregulation of cGMP phosphodiesterase induced by expression of GTPase-deficient cone transducin in mouse rod photoreceptors. Invest Ophthalmol Vis Sci. 1994; 35: 2932–2947. PMID: 8206711

42. Sjöstrand FS, Elfvin LG. Some observations on the structure of the retinal receptors of the toad eye as revealed by the electron microscope. In: Rhodin JAG, Sjöstrand FS, editors. European Regional Conference on Electron Microscopy 1956: Electron Microscopy: Proceedings of the Stockholm Conference; 1956 Sept 17–20; Stockholm, Sweden. Uppsala: Almqvist & Wiksells; 1957. p. 194–196.

43. Doan T, Azevedo AW, Hurley JB, Rieke F. Arrestin competition influences the kinetics and variability of the single-photon responses of mammalian rod photoreceptors. J Neurosci. 2009; 29: 11867–11879. https://doi.org/10.1523/JNEUROSCI.0819-09.2009 PMID: 19776273

44. Liebman PA, Entine G. Lateral diffusion of visual pigment in photoreceptor disk membranes. Science. 1974; 185: 457–459. https://doi.org/10.1126/science.185.4149.457 PMID: 4546260

45. Wey CL, Cone RA, Edidin MA. Lateral diffusion of rhodopsin in photoreceptor cells measured by fluorescence photobleaching and recovery. Biophys J. 1981; 33: 225–232. https://doi.org/10.1016/S0006-3495(81)84883-7 PMID: 6971659

46. Govardovskii VI, Korenyak DA, Shukolyukov SA, Zueva LV. Lateral diffusion of rhodopsin in photoreceptor membrane: a reappraisal. Mol Vis. 2009; 15: 1717–1729. PMID: 19727341

47. Wang Q, Zhang X, Zhang L, He F, Zhang G, Jamrich M, et al. Activation-dependent hindrance of photoreceptor G protein diffusion by lipid microdomains. J Biol Chem. 2008; 283: 30015–30024. https://doi.org/10.1074/jbc.M803953200 PMID: 18713731

48. Fotiadis D, Liang Y, Filipek S, Saperstein DA, Engel A, Palczewski K. Atomic-force microscopy: Rhodopsin dimers in native disc membranes. Nature. 2003; 421: 127–128. https://doi.org/10.1038/421127a PMID: 12520290

49. Bayburt TH, Leitz AJ, Xie G, Oprian DD, Sligar SG. Transducin activation by nanoscale lipid bilayers containing one and two rhodopsins. J Biol Chem. 2007; 282: 14875–14881. https://doi.org/10.1074/jbc.M701433200 PMID: 17395586

50. Whorton MR, Jastrzebska B, Park PSH, Fotiadis D, Engel A, Palczewski K, et al. Efficient coupling of transducin to monomeric rhodopsin in a phospholipid bilayer. J Biol Chem. 2008; 283: 4387–4394. https://doi.org/10.1074/jbc.M703346200 PMID: 18033822

51. Bayburt TH, Vishnivetskiy SA, McLean MA, Morizumi T, Huang CC, Tesmer JJG, et al. Monomeric rhodopsin is sufficient for normal rhodopsin kinase (GRK1) phosphorylation and arrestin-1 binding. J Biol Chem. 2011; 286: 1420–1428. https://doi.org/10.1074/jbc.M110.151043 PMID: 20966068

52. Vishnivetskiy SA, Ostermaier MK, Singhal A, Panneels V, Homan KT, Glukhova A, et al. Constitutively active rhodopsin mutants causing night blindness are effectively phosphorylated by GRKs but differ in arrestin-1 binding. Cell Signal. 2013; 25: 2155–2162. https://doi.org/10.1016/j.cellsig.2013.07.009 PMID: 23872075

53. Tsukamoto H, Sinha A, DeWitt M, Farrens DL. Monomeric rhodopsin is the minimal functional unit required for arrestin binding. J Mol Biol. 2010; 399: 501–511. https://doi.org/10.1016/j.jmb.2010.04.029 PMID: 20417217

54. Zhuang T, Chen Q, Cho MK, Vishnivetskiy SA, Iverson TM, Gurevich VV, et al. Involvement of distinct arrestin-1 elements in binding to different functional forms of rhodopsin. Proc Natl Acad Sci USA. 2013; 110: 942–947. https://doi.org/10.1073/pnas.1215176110 PMID: 23277586

55. Hanson SM, Gurevich EV, Vishnivetskiy SA, Ahmed MR, Song X, Gurevich VV. Each rhodopsin molecule binds its own arrestin. Proc Natl Acad Sci USA. 2007; 104: 3125–3128. https://doi.org/10.1073/pnas.0610886104 PMID: 17360618

56. Kang Y, Kuybeda O, de Waal PW, Mukherjee S, Van Eps N, Dutka P, et al. Cryo-EM structure of human rhodopsin bound to an inhibitory G protein. Nature. 2018; 558: 553–558. https://doi.org/10.1038/s41586-018-0215-y PMID: 29899450

57. He Y, Gao X, Goswami D, Hou L, Pal K, Yin Y, et al. Molecular assembly of rhodopsin with G protein-coupled receptor kinases. Cell Res. 2017; 27: 728–747. https://doi.org/10.1038/cr.2017.72 PMID: 28524165

58. Kang Y, Zhou XE, Gao X, He Y, Liu W, Ishchenko A, et al. Crystal structure of rhodopsin bound to arrestin by femtosecond X-ray laser. Nature. 2015; 523: 561–567. https://doi.org/10.1038/nature14656 PMID: 26200343

59. Zhou XE, He Y, de Waal PW, Gao X, Kang Y, Van Eps N, et al. Identification of phosphorylation codes for arrestin recruitment by G protein-coupled receptors. Cell. 2017; 170: 457–469. https://doi.org/10.1016/j.cell.2017.07.002 PMID: 28753425

60. Rieke F, Baylor DA. Molecular origin of continuous dark noise in rod photoreceptors. Biophys J. 1996; 71: 2553–2572. https://doi.org/10.1016/S0006-3495(96)79448-1 PMID: 8913594

61. Cohen AI. New details of the ultrastructure of the outer segments and ciliary connectives of the rods of human and macaque retinas. Anat Rec. 1965; 152: 63–79. https://doi.org/10.1002/ar.1091520108 PMID: 14316821

62. Bialek W, Owen WG. Temporal filtering in retinal bipolar cells. Elements of an optimal computation? Biophys J. 1990; 58: 1227–1233. https://doi.org/10.1016/S0006-3495(90)82463-2 PMID: 2291942

63. Sampath AP, Strissel KJ, Elias R, Arshavsky VY, McGinnis JF, Chen J, et al. Recoverin improves rod-mediated vision by enhancing signal transmission in the mouse retina. Neuron. 2005; 46: 413–420. https://doi.org/10.1016/j.neuron.2005.04.006 PMID: 15882641

64. Lasansky A. Contacts between receptors and electrophysiologically identified neurones in the retina of the larval tiger salamander. J Physiol (Lond). 1978; 285: 531–542.

65. Borges S, Wilson M. Structure of the receptive fields of bipolar cells in the salamander retina. J Neurophysiol. 1987; 58: 1275–1291. https://doi.org/10.1152/jn.1987.58.6.1275 PMID: 3437334

66. Tsukamoto Y, Morigiwa K, Ueda M, Sterling P. Microcircuits for night vision in mouse retina. J Neurosci. 2001; 21: 8616–8623. https://doi.org/10.1523/JNEUROSCI.21-21-08616.2001 PMID: 11606649

67. Wu SM. Synaptic transmission from rods to bipolar cells in the tiger salamander retina. Proc Natl Acad Sci USA. 1985; 82: 3944–3947. https://doi.org/10.1073/pnas.82.11.3944 PMID: 2987955

68. Capovilla M, Hare WA, Owen WG. Voltage gain of signal transfer from retinal rods to bipolar cells in the tiger salamander. J Physiol (Lond). 1987; 391: 125–140.

69. Berntson A, Smith RG, Taylor WR. Transmission of single photon signals through a binary synapse in the mammalian retina. Vis Neurosci. 2004; 21: 693–702. https://doi.org/10.1017/S0952523804215048 PMID: 15683557

70. Field GD, Rieke F. Mechanisms regulating variability of the single photon responses of mammalian rod photoreceptors. Neuron. 2002; 35: 733–747. https://doi.org/10.1016/s0896-6273(02)00822-x PMID: 12194872

71. Sampath AP, Rieke F. Selective transmission of single photon responses by saturation at the rod-to-rod bipolar synapse. Neuron. 2004; 41: 431–443. https://doi.org/10.1016/s0896-6273(04)00005-4 PMID: 14766181